Talanta 85 (2011) 35–42

Contents lists available at ScienceDirect

Talanta

journal homepage: www.elsevier.com/locate/talanta

Biosensors elaborated on gold nanoparticles, a PM-IRRAS characterisation of the IgG binding efficiency

Anne-Laure Morel[a,b], Souhir Boujday[a,b], Christophe Méthivier[a,b], Jean-Marc Krafft[a,b], Claire-Marie Pradier[a,b,*]

[a] Université Pierre et Marie Curie, Paris 6, UMR CNRS 7197, Laboratoire de Réactivité de Surface, F75005 Paris, France
[b] CNRS, UMR 7197, Laboratoire de Réactivité de Surface, F75005 Paris, France

ARTICLE INFO

Article history:
Received 6 October 2010
Received in revised form 11 February 2011
Accepted 20 February 2011
Available online 24 February 2011

Keywords:
Gold nanoparticles
Immunosensors
AFM
PM-IRRAS
SERS

ABSTRACT

This work is focused on studying the grafting of gold nanoparticles (Np) on a cystamine self-assembled monolayer on gold, in order to build sensitive immunosensors. The synthesis and deposition of gold nanoparticles, 13 and 55 nm sizes, were characterised by combining Polarisation Modulation Infrared Reflection–Absorption Spectroscopy (PM-IRRAS), X-ray Photoelectron Spectroscopy (XPS) Surface Enhanced Raman Scattering (SERS), and Atomic Force Microscopy (AFM) which all indicated the formation of a dispersed layer of nanoparticles. This observation is explained by the compromise between the high reactivity of amine-terminated layers towards gold, and interparticle repulsions. Nps were then functionalised with antibody probes, and the recognition by an anti-rIgG was assayed both on planar and Np gold surfaces.

The important result is that nanoparticles of 55 nm are preferable for the following reasons: they enable to build a denser and well dispersed layer and they increase both the number of receptors (IgGs) and their accessibility. Beside these geometric improvements, a net enhancement of the Raman signal was observed on the 55 nm nanoparticle layer, making this new platform promising for optical detection based biosensors.

1. Introduction

The use of gold nanoparticles (AuNps) is particularly attractive in biological and medical fields for imaging or optical detection enhancement thanks to the unique properties of surface plasmon resonance (SPR) and resonance light scattering, while they are biocompatible and easily chemically modified [1]. After recalling the principle of bioconjugate chemistry on gold, as well as of AuNp-based techniques like SPR and SERS, Astruc and Boisselier describe, in a recent review, the fantastic interest of AuNps for medical diagnosis and therapeutic applications [2]. As an example, AuNps, conjugated to antibodies, may be used as cancer biomarkers; alternatively, they may be stabilized by dendrimers thus leading to supramolecular properties applicable to encapsulation or specific substrate-specific interactions [3]. Recent developments in the synthesis and optical properties of gold nanoparticles are given in reference [4].

Gold nanoparticles have been used for improving the sensitivity of biosensors thanks to their optical properties or because they enable easy electrochemical detection of biomolecular recognition phenomena [5]. Various procedures to modify electrodes by gold NPs have been implemented and compared, showing the interest of immobilising AuNp on thiol monolayers [6,7], or using Nps assembled on a polymer grafted on an electrode [8]. Another example reports the construction of an amperometric immunosensor on a mixed NH_3^+/SH-terminated SAM layer, modified with gold Nps, taking advantage of the high affinity of gold to either of these two functions [9]. Antibodies are subsequently directly immobilised on the gold Nps, by simple incubation in an antibody solution, resulting in an efficient immunosensor for α-fetoprotein; the enhanced number and accessibility of probes were mentioned but not measured in this case [6].

In a very pioneer work, Natan and co-workers demonstrated the possibility to take advantage of the electronic coupling between gold planar films and gold nanoparticles to obtain larger changes in reflectivity and, thus, amplified SPR signals [10]. More recently, gold nanoparticles were immobilised on a dithiol layer or within a protein–polymer mixture, both methods resulting in the enhanced sensitivity of surface plasmon resonance biosensors [11,12]. The interest of building an immunosensor on gold nanoparticles, in particular the increase of the number of molecular receptors

* Corresponding author at: Université Pierre et Marie Curie, Paris 6, UMR CNRS 7197, Laboratoire de Réactivité de Surface, F75005 Paris, France.
Tel.: +33 1 44 27 55 33.
E-mail address: claire-marie.pradier@upmc.fr (C.-M. Pradier).

0039-9140/$ – see front matter © 2011 Elsevier B.V. All rights reserved.
doi:10.1016/j.talanta.2011.02.028

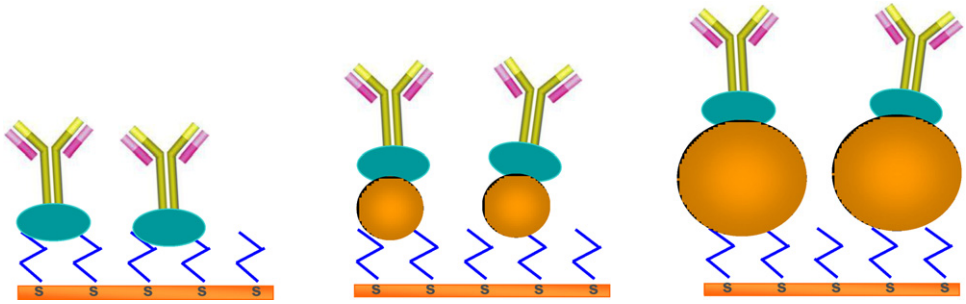

Scheme 1. Schematic representation of the 3D immunosensor built on a cystamine layer or gold nanoparticles; for sake of clarity, the respective sizes of the nanoparticles and chemicals are not at the right scale.

and of their accessibility, was also mentioned in reference [13].

Gold Nps, combined with a SiO_2 interface were shown to enhance plasmon coupling and thus SPR sensor sensitivity [14]. Even the gold Np colour change, when aggregated, was used for assaying DNA hybridisation [15].

Eventually, surfaces modified by gold nanoparticles have been applied to bioanalysis taking advantage of the high sensitivity of Surface Enhanced Raman Scattering (SERS) on such structures [16]. Recent papers made clear the complex interplay of the particle size, shape, as well as distance to the substrate, upon SERS intensity [17,18].

Though not exhaustive, this short overview of some AuNp-based immunosensors shows the huge interest of such nanostructured sensing platforms. Among the multiple interest of using AuNps, it is difficult to isolate, and thus optimise, the possible causes of signal enhancement, increase of the receptor number, of their accessibility, or gain of sensitivity due to the remarkable physical/optical properties of gold Nps for example.

In the present paper, we thus focus on the preparation and grafting of gold nanoparticles of various sizes on an amine-terminated Self-Assembled Monolayers (SAMs), and their applications as new platforms for building sensitive immunosensors following Scheme 1. The number and accessibility of the immobilised molecular probes, rabbit immunoglobins (rIgG), will be estimated on three different systems, (i) a planar gold surface, (ii) 13 nm or (iii) 55 nm nanoparticles immobilised on a gold surface. To do so, the Np layers will be characterised by combining Polarisation Modulation InfraRed Reflection Absorption Spectroscopy (PM-IRRAS), Photoelectron Spectroscopy (XPS), Atomic Force microscopy (AFM) and SERS; the anti-rIgG recognition reaction will be measured by PM-IRRAS a technique which enables a strict comparison of the numbers of immobilised probes or target molecules without any optical or electrical effect.

2. Experimental

2.1. Materials

$HAuCl_4$ (99.5%) was purchased from Merck (Darmstadt, Germany). 1-Mercapto-11-undecanoic acid (MUA), *N*-hydroxysuccinimide (NHS), *N*-1-(3-dimethylaminopropyl)-*N*′-ethylcarbodiimide hydrochloride (EDC), Ethanolamine, trisodium citrate, cystamine dihydrochloride (98%) (CA) were obtained from were purchased from Aldrich (France). Rabbit IgG (rIgG), goat anti-rabbit IgG (anti-rIgG), goat serum, bovine serum albumin, (BSA) and recombinant protein A (PrA) were purchased from Sigma. All solvents were reagent-grade and used without any further purification.

Planar gold samples were glass substrates (11 mm × 11 mm) coated with a 2.5 nm thick chromium layer and a 200 nm thick gold layer (Arrandee, Werther, Germany). The clean gold chips were annealed in a butane flame to ensure a good crystallinity of the topmost layers, as recommended by the company.

2.2. Gold nanoparticle synthesis and characterisation

The gold nanoparticles were prepared by reducing $HAuCl_4$ in a trisodium citrate aqueous solution according to a previously published route [19,20]. The two following stock solutions were prepared from pure water, 1 mM $HAuCl_4$ and 38.8 mM trisodium citrate in pure water; 50 mL of 1 mM $HAuCl_4$ solution was heated to boiling with vigorous stirring, and 5 mL of the Na_3-citrate solution were added rapidly resulting in a colour change from pale yellow to red-wine. The nanoparticle size was tuned by changing the citrate/Au molar ratio as first described by Frens [21]. As an example, 1.3 mL of 38.8 mM Na_3-citrate solution was used to obtain nanoparticles of ca 60 nm diameter. After boiling for 15 min, the heating mantle was removed, and stirring was continued for an additional 15 min. After the solution reached room temperature, it was kept at +4 °C.

The resulting colloidal solution was characterised by UV–visible spectroscopy, and by Transmission Electron Microscopy.

- Gold Np sizes were visualised using a JEOL transmission electron microscope operating at 100 kV. Samples were prepared by evaporating microdrops of nanoparticle solution (25 °C) on Formvar-coated copper grids

2.3. Gold surface functionalisation and protein immobilisation

Before gold Np grafting, gold samples were immersed in a 10 mM aqueous CA solution during 12 h, then washed three times in pure water and dried under nitrogen flow. After that, substrates were immersed in 10 mL freshly prepared colloidal solution for 1 h, then washed once in pure water, and dried under nitrogen flow. Planar gold surfaces and gold nanoparticles-derived platforms were then submitted to an identical protocol in order to build immunosensing surfaces; they were first immersed in a 10 mM mercapto-11-undecanoic (MUA) solution in ethanol, in order to graft accessible acidic functions. On gold nanoparticles, the objective was to replace citrate ligands by acid-terminated thiols. After 3 h, the substrates were washed 3 times in the same volume of EtOH and dried under nitrogen flow. The acidic functions were activated with a solution of NHS (60 mM) and EDC (30 mM) in water for 1 h 30 then, 150 μL of a solution of PrA (50 and 100 mg/L) in PBS (pH 7.4) was deposited. After 1 h, substrates were washed three times with PBS. Then a drop of 1 M ethanolamine in water was deposited onto the samples in order to deactivate residual ester functions. After 20 min, they were rinsed once in water and dried under nitrogen flow. To block non specific binding sites, a microdrop of a 50 mg L^{-1} solution of BSA in PBS was deposited for 30 min. After rinsing 3

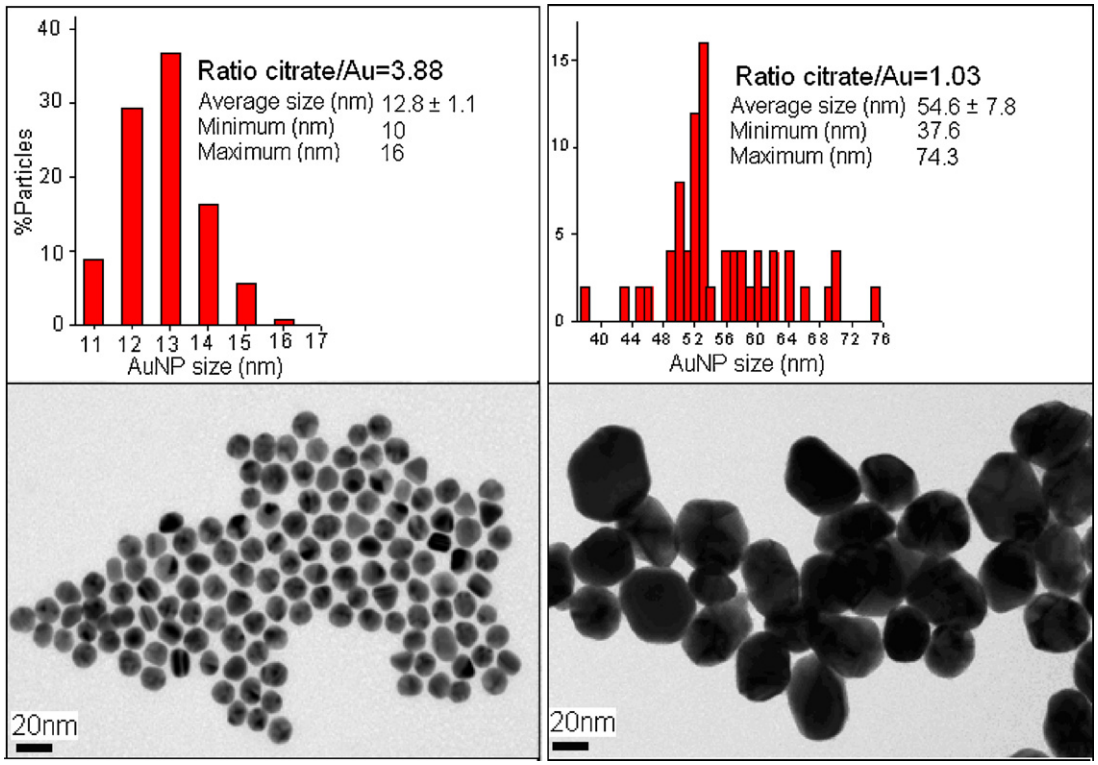

Fig. 1. TEM images of the two sets of nanoparticles deposited on a copper grid.

times in PBS, solutions of rIgGs (50 and 100 mg/L) were added by depositing a drop onto the substrates during 1 h and washed again in PBS. The antibody accessibility was checked by reacting a secondary anti-rIgG (50 mg L^{-1} in PBS, 1 h), then washing 3 times in PBS.

2.4. Surface characterisation

Au substrates were characterised by Polarisation Modulation-Infrared Refection Absorption Spectroscopy (PM-IRRAS), Photoelectron Spectroscopy (XPS), at each step of their modification; Surface Enhanced Raman Scattering (SERS) spectra, as well as AFM images were recorded after nanoparticle grafting.

- PM-IRRAS was performed using an experimental setup already described in a previous paper [22]. The technique is sensitive to the vibrations of adsorbed monolayers as well as those of proteins immobilised in the vicinity of the surface.
- XPS measurements were done using a Phoibos MCD 150 X-ray photoelectron spectrometer from SPECS (Germany), equipped with a non-monochromatized magnesium X-ray source ($h\nu$ = 1253.6 eV) powered at 10 mA and 15 kV, and a Phoibos 150 hemispherical energy analyzer without charge stabilisation device at a take-off angle of 90°. A pass energy of 10 eV, was used for narrow scans of the O 1s, C 1s, Au 4f, N 1s and S 2p regions. The binding energy scale was calibrated by fixing the C 1s component due to carbon only bound to carbon and hydrogen at 284.8 eV. The data treatment was performed with the Casa XPS software (Casa Software Ltd., UK). Unless stated otherwise, the peaks were decomposed using a linear baseline, and a component shape defined by the product of a Gauss and a Lorentz function, in the 70:30 ratio. Molar concentration ratios were calculated using peak areas normalised according to Scofield factors [23].
- AFM images were recorded with a commercial diCaliber AFM microscope from VEECO Instruments Inc. Topographic images were taken in non-contact dynamic mode also known as tapping® mode. Silicon nitride tips (resonance frequency of ~280–400 kHz, and a spring constant of 20–80 N/m) have been used. Images were obtained at a constant speed of 2 Hz with a resolution of 512 lines of 512 pixels each. The raw data were processed using the imaging processing software di SpmLabAnalysis from Veeco Instruments Inc.
- Raman-SERS experiments were performed on a commercial Raman spectrometer (Model HL5R of Kaiser Optical Systems, Inc.). Surface Enhanced Raman Scattering spectra were recorded in the 100–3450 cm^{-1} range on a spectrometer (Model HL5R of Kaiser Optical Systems, Inc.) connected to a microscope (Olympus, objective: 100×). It is equipped with a high-powered near-IR laser diode working at 785 nm. The optical microscope was used to focus the laser beam. Each SERS analysis was the result of 20 acquisitions of 30 s at 20 mW.

3. Results and discussion

3.1. Synthesis and characterisation of AuNps

After preparation of the colloidal gold nanoparticle solutions, the size, and dispersity of the resulting nanoparticles were estimated from UV–visible characterisation of the solution, and Transmission Electron Microscopy (TEM) analyses.

The results of UV characterisation are given as a supplementary data.

TEM images, shown in Fig. 1, enable to estimate the Np size with reasonable accuracy; one sees two that two sets of nanoparticles have been indeed obtained, the average calculated sizes being 12.8 ± 1.1 and 54.6 ± 7.8 nm respectively; they will be noted 13 and 55 nm Nps in the following. Note the very narrow size dispersion of AuNps in the case of the smallest ones (d = 13 nm), whereas more

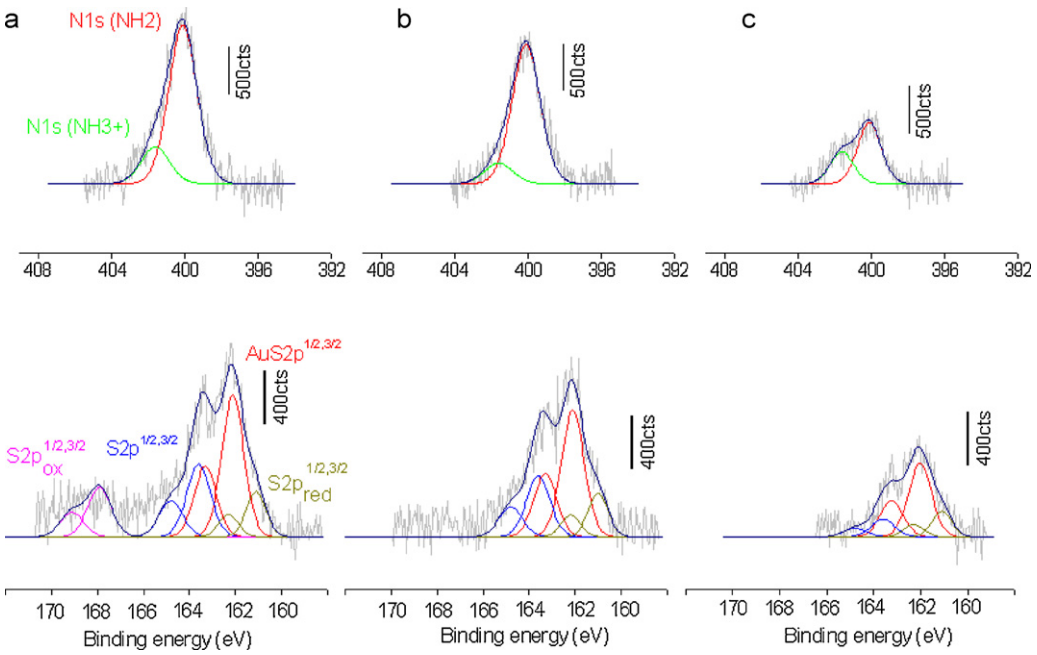

Fig. 2. XPS spectra, (A) N 1s and (B) S 2p regions of the surface (a) after CA grafting, after CA + Au Np deposition, (b) 15 and (c) 60 nm.

size and shape heterogeneities were observed for larger AuNps. These results allow us to use these two sets of nanoparticles for testing the nanostructured sensing systems.

3.2. Grafting and characterisation of the cystamine (CA) layer, and of the AuNps grafted on a CA layer

XPS was used to characterise the gold-coated samples after CA grafting (step 1) and after gold Np immobilisation (step 2).

After step 1, the XPS analysis reveals the presence of nitrogen, sulfur and carbon at the surface. The N 1s peak, strongly asymmetric, (Fig. 2a, upper spectra) could be decomposed into two contributions, at 400.1 and 401.6 eV indicating the coexistence of neutral and protonated amine groups on the surface. This is in agreement with results obtained by other authors [24]. This CA layer displays NH_2 or NH_3^+ functions, both being known to have affinity to ligand-surrounded gold nanoparticles; in particular, favourable electrostatic interactions between NH_3^+ and citrates may be reasonably expected.

The sulfur peak is shown in Fig. 2a, lower spectra; four doublets were necessary to fit it at best; one main doublet with the S $2p_{3/2}$ contributions at 162.1 eV, and a smaller one with the S $2p_{3/2}$ at 163.7 eV; this reveals the coexistence of both sulfur atoms bound to gold (signal at 162.1 eV), and unbound or disulfide sulfur involved in SH or S–S bonds for the second doublet [25]. The existence of the latter sulfur species may be explained by CA molecules linked to the CA layer via interchain interactions, rather than by forming S–Au bond; a third component, rather weak, at the lowest binding energy (S $2p_{3/2}$ = 161.1 eV) is more difficult to ascribe; it has already been observed by Wirde et al., upon adsorption of cystamine, cysteamine or alcanethiols, and attributed to a sulphur, highly coordinated to Au surface atoms, and resulting from a reorganisation of the adsorbed layer [24].

Eventually, another, very weak, S 2p doublet appears at 167.8 eV after the formation of CA SAMs, which may be due to the formation of oxidized sulfur species, such as sulfonates or sulfinates [24]. These oxidized species, likely negatively charged, may be retained in the adsorbed film even after washing, due to the electrostatic interactions with the positively charged amino groups.

Note that we also tested the formation of the same amine-terminated layer, but from cysteamine solutions. The same four components were observed in the S 2p peak (spectrum not shown); however, the low BE one was very weak, again in agreement with Wirde's work and confirming our attributions.

Aqueous solutions of nanoparticules, 13 nm and 55 nm size, were then let to interact with such CA-modified gold surfaces.

XPS analyses of the gold chips after Np grafting showed an attenuation of the sulfur contribution of ca 25% and 65% for the 13 and 55 nm Nps respectively, suggesting that no more than one fourth of the surface was covered with 13 nm Nps, while almost two third were covered with 55 nm Nps and their ligands. The profile of the S 2p and N 1s peaks hardly changed upon Np grafting (Fig. 2b and c). The absence of a contribution at 168 eV, on these latter spectra, suggests that sulfur oxidized species are displaced upon grafting the gold NPs.

The very low coverage, observed with 13 nm particles, rarely mentioned in the literature likely originates from the strongly repulsive interparticle interactions due to citrate ligands which are known to prevent Np aggregation [26]. As for the 55 nm particles, the surface coverage appears to be higher, the main reason being a geometric one (bigger nanoparticles!); another contributing factor is that, despite the presence of ligands, some aggregates were formed in the colloidal solution during their preparation.

Grafting of Nps on the CA layer was evidenced by the PM-IRRAS analysis of the gold surface, thanks to the appearance of bands at 1260, 1110 cm^{-1} ascribed to the ν(C–O) and δOH bands of the citrate ligands respectively (see IRRAS spectra, and spectral data, in Supplementary data).

Fig. 3 shows the Raman spectra of a CA salt powder, of a solution of trisodium citrate, and of a gold surface after gold Np grafting (SERS spectra). The two upper spectra, i.e. the gold planar surface after step 2, reveal the bands characteristic of the CA underlayer, which were not visible after step 1, and the fingerprints of the citrates; this result confirms the presence of nanoparticles thanks to the chemical signature of their ligands, only visible because of the SERS effect induced by these nanostructures; note that this also permits the detection of the CA molecules. The list of bands and their attribution are given in Table 1.

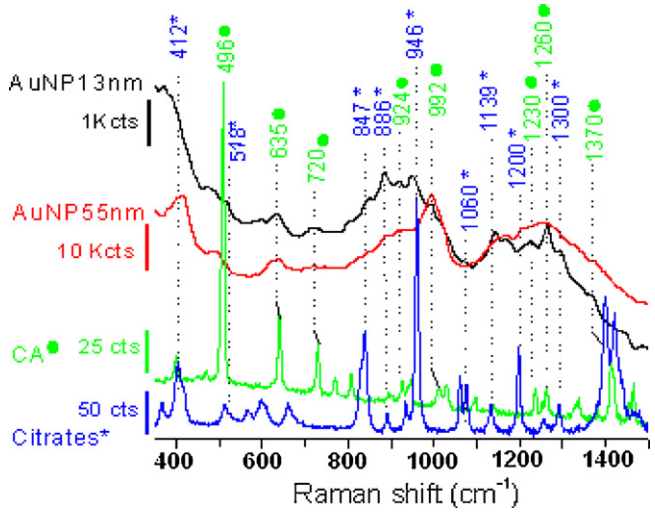

Fig. 3. Raman spectra of the neat cystamine and of citrate solution (lower spectra), and SERS spectra of the gold-CA surface after deposition of a gold particle layers, 13 and 55 nm (upper spectra).

SERS spectra can be decomposed into two main regions. The ν(C–S) region, between 600 and 750 cm^{-1}, which includes data about the C–S bond close to the metal, and the ν(C–C) region between 1000 and 1200 cm^{-1}, including the vibrations of the carbon chain.

In the first region, one can observe the ν(C–S) vibration bands, at 635 and 720 cm^{-1} corresponding to the gauche and trans conformers respectively. The intensity ratio of these two bands, I_G/I_T, is a probe of the quality of the monolayer. It is in the present case, lower than unity, suggesting that the gauche conformers are dominating, probably favoured by the possible interaction of both the SH and NH_2 end-groups of the CA molecules with the gold surface [29]. This conformation is obviously not favourable to the Np grafting. We also observe that the ν(C–S) signals undergo a red shift of ca 10 cm^{-1} likely due to an electron transfer from the molecule to the gold surface [30,31].

In the second region, one can observe a massif of bands around 900–1000 cm^{-1} corresponding to the C–C bonds from cystamine and citrates. Note that the C–C stretch, coupled to the C–N vibrations of the cystamine, appears at 992 cm^{-1}, slightly shifted compared to the neat CA spectrum, either due to some electron transfer to the metal again or to a change in the conformation of cystamine [29,32].

Table 1
SERS signals and their attribution.

Raman shift (cm^{-1})	Assignments
412	ν(C–C)*
496	ν(S–S)
518	δ(C–C)*
635	$\nu(C–S)_G$
720	$\nu(C–S)_T$
847	ν_s(C–O)*
886	ν(C–C)*
924	ν(C-C)
946	ν(C–COO^-)*
992	ν(C–C(–N))
1060	ν(C–O)*
1139	$\nu(C–C)_{T*}$
1200	$\nu(C–C)_{T*}$
1230	$CH_{2\ wag}$
1260	δ(C–H)
1300	δ(C–H)*
1370	ν_s(COO)*

The star refers to the citrate characteristic bands.

Other vibration bands, at 1230, 1260, 1300 cm^{-1}, confirm the presence of carboxylates coming form the AuNPs. The intense symmetric stretching mode ν_s(COO) of citrates, at ca 1400 cm^{-1} on the pure citrate, appears at 1370 cm^{-1} on the SERS spectra, indicating interactions of the carboxylate groups with the surface [33].

Note that the SERS enhancement factor for the 55 nm gold Nps is 10 times higher than for the smaller ones. This may be explained by the complex interplay of the interparticle distance, the size and the shape of the nanoparticles which all contribute to SERS intensity [27]. The distance between the 55 nm NPs is smaller for geometric reasons, and the coverage higher, than for 13 nm NP as calculated from XPS data. Moreover, as seen in TEM, 55 nm NPs are not all spherical; size and shape heterogeneities may create an increase of the SERS intensity by the enhancement of the localised electromagnetic field resulting from the coupling of longitudinal and transversal surface plasmon [28].

Eventually, AFM was used to characterise the morphologies of the surface after Np grafting. Fig. 4A shows AFM images obtained upon 13 nm Np grafting on CA. One observes a well dispersed layer of gold nanoparticles, likely thanks to the citrate ligands that prevent aggregation. Some aggregates could however been observed, but these are rare and limited to two Nps (Fig. 4A, b). The line scan (Fig. 4A, a), making clear bumps of ca 13 nm height, confirms the grafting of well dispersed nanoparticles. A simple glance at the AFM image indicates that the gold surface is far from being totally covered; gold terraces of the pristine surface are still distinguishable. The AuNp density has been estimated by counting the number of 13 nm AuNPs on a 500 nm line. A 100% coverage rate would correspond to ca 30 15 nm AuNPs. Here 4–5 AuNPs appear along the selected profile, i.e. 5 times less than a full coverage, not taking into account the few aggregated AuNps on the sample; this is in good agreement with the 25% coverage calculated from XPS data.

AFM image of 55 nm Np/CA surface is shown on Fig. 4B. This image shows a denser layer of nanoparticles. Gold terraces are no more visible; moreover, there are some aggregates i.e. some Nps on top of the first layer of Nps as shown by the line scan of Fig. 5B, b. The average line scan (Fig. 4B, a) confirms the size of isolated nanoparticles, ca 55 nm, and shows 4–5 AuNPs on a 500 nm line. This corresponds to 50–62% of a full monolayer, rather close to the number calculated from XPS. The 500 nm line scan also suggests that the interparticle distance between 55 nm AuNps is smaller than the 13 nm AuNps, and this is likely a determining factor for the enhanced SERS intensity on the larger particle layer.

At that point, let us recall that we previously realised similar Np-based immunosensors, by grafting 13 nm Au Nps on an hexanedithiol layer; gold Nps were indeed well grafted, but at a very low coverage that we attributed to the formation of dithiol bridging molecules, resulting from interaction of both ends with the planar surface [34].

3.3. Elaboration and test of immunosensors on planar and Np gold surfaces

Flat gold surfaces, and gold Nps deposited on the gold wafers, were similarly functionalised, following the procedure described in the experimental section, in order to immobilise antibody receptor molecules, rIgGs, and compare the efficiencies of the anti-rIGg recognition assays.

Before building planar and Np-based immunosensors, the concentrations of PrA and rIgG have been varied and tested regarding their recognition efficacy. On planar immunosensors, as well as on 13 nm Np immunosensors, the optimised concentrations of PrA and rIgG were found to be 50 mg/L; these values corresponded to saturation concentrations for both of them, with the highest PrA/IgG and anti-IgG/rIgG ratios. On the 55 nm Np immunosensors, the optimised concentrations of PrA and rIgG were 50 mg/L

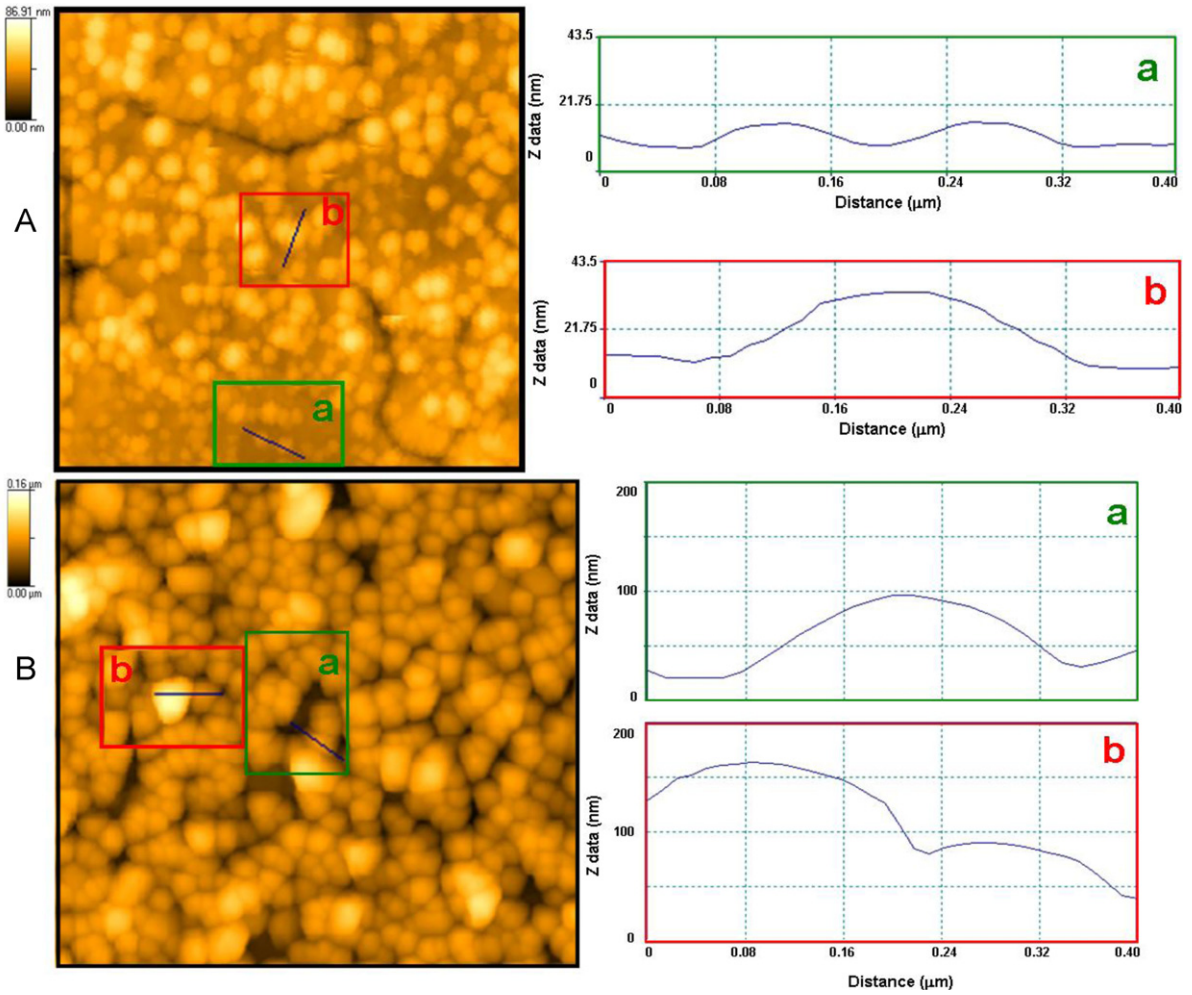

Fig. 4. topographic AFM images, and associated scan lines of the gold surface after deposition of the gold nanoparticles, 13 nm (Fig. 4A, upper image) and 55 nm (Fig. 4B, lower image).

and 100 mg/L respectively. These values corresponded to a good compromise between a maximal amount of rIgG, and their best accessibility.

The successive steps of the immunosensor elaboration, as well as the detection reactions, were evaluated from the amide band variations.

Fig. 5 (left) shows the amide band IR region of the 55 nm Nps-modified surfaces after being submitted to rIgG, BSA, and anti-rIgG solutions and rinsing in pure water after each step; similar series of spectra were obtained on the two other sensing platforms (planar gold and 13 nm Nps). Fig. 5 (right) shows the evolution of the total amide IR region intensity, at each step, for the three studied systems.

The amide band intensity increases at each step confirming the successive binding of each type of proteins; note that submitting the samples to BSA solution after PrA binding induces

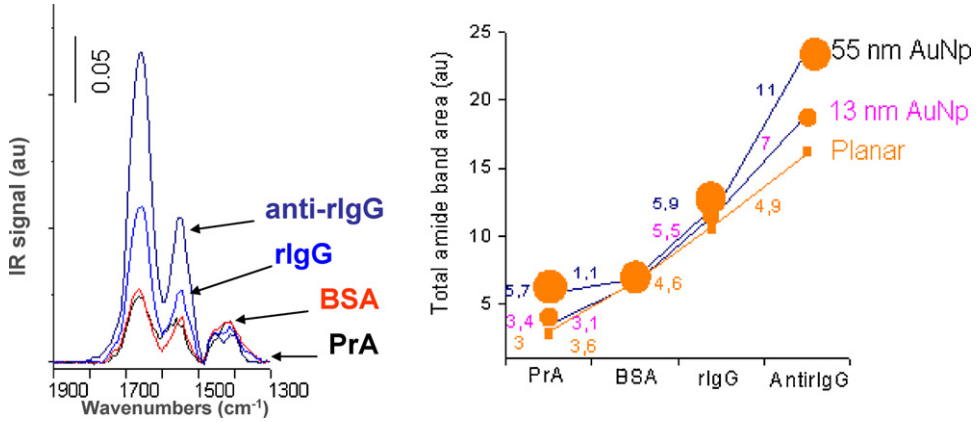

Fig. 5. Left: IR spectra at each step of elaboration and test of the immunosensor built on 55 nm AuNps. Right: IR intensity in the amide region (1450–1750 cm^{-1}) at each step of protein grafting on the three studied immunsensors.

Table 2
Estimation of the amount of PrA and rIgG grafted on planar, 13 nm AuNP, and 55 nm AuNP based immunosensors obtained by IR. Calculation of the IgG/PrA and anti-IgG/IgG ratios.

	PrA amount (IR band area)	IgG amount (IR band area)	Anti-rIgG amount (IR band area	IgG/PrA Molecular amount	Anti-rIgG/rIgG Molecular amount
Planar	3	4.6	4.9	0.5	1.1
13 nm	3.4	5.5	7.0	0.5	1.3
55 nm	5.7	5.9	11.0	0.3	1.9

some albumin adsorption which is expected to block all surface sites against non specific adsorption of rIgGs. By correcting the amide band areas by the molecular weight of each protein, 150 kDa and 44.6 kDa for IgG and PrA, respectively [35], one can advantageously compare the immobilized molecular amounts of the various proteins. The results are shown in Table 2.

Without Nps, the rIgG over PrA ratio, and anti-rIgG over rIgG ratio, were equal to 0.5 and 1.1 respectively, showing a rather low level of antibody binding to protein A. Indeed, Protein A contains four high-affinity binding sites for the Fc region of IgGs [35–37]. The binding capacity of immobilized PrA reported in the literature varies in the 0.2–1.0 range [35,38,39]. The anti-rIgG over rIgG ratio equal to 1.1 indicates a reasonable recognition efficiency (the maximum would be 2).

With 13 nm Au Nps, one sees a slight increase of IR band intensities at each step; slightly more PrA molecules are adsorbed onto the CA layer but no change is observed in their binding capability. More interesting the anti-rIgG over rIgG ratio passes from 1.1 to 1.3. These rather low differences between planar gold surfaces and 13 nm AuNps are understandable when considering first, that nanoparticles are very small; the available surface area, assuming that half of the spherical nanoparticles are not accessible, and a surface coverage of 25%, is only increased by a factor of 1/4; second, these Nps are linked to the surface via a very thin CA layer, in other words, they are almost stuck to the surface thus preventing the accessibility to the underneath side, i.e. an actual 3D effect.

With 55 nm Nps, the IR band changes suggest a much better enhancement of both the number of receptors and of their accessibility. Despite the fact that they are also attached to a thin CA layer, the number of bound PrA molecules was almost multiplied by a factor of 2; it might be interesting to note that the amount of BSA blocking proteins was significantly lower than in the previous cases, where a non-specific irreversible adsorption of BSA was observed; this indicates a higher quality of the PrA layer on the largest nanoparticle layer; the amount of rIgGs was increased and, more important, the rIgG accessibility, attested by the anti-rIgG over rIgG ratio, was also improved by a factor close to two; all these data are summarised in Table 2. This improvement suggests that, at each step, a compromise has to be found between an increase the number of receptors, and a risk of decreasing their accessibility.

4. Conclusion

The synthesis of gold Nps of controlled size and dispersion has permitted to elaborate two different nanoparticle-based immunosensors. Gold Nps of 13 or 55 nm size were synthesised and deposited on a cystamine monolayer grafted to a planar gold chip. Evidenced by various characterisation techniques, the layer of 55 nm nanoparticles leads to the most intense enhancement of the SERS signal. In a further step, gold Nps were successfully used as plate-forms to attach antibody receptors. In comparison with SAMs without Nps grafting, the 3D immunosensors elaborated in this work display an improvement of the number of receptor molecules, the rIgGs, and of their accessibility. Moreover, the evidenced SERS enhancement on the 55 nm Nps elaborated in this work gives much hope for further works focussed on biosensors based on Raman-SERS or on other optical techniques like surface plasmon resonance.

Acknowledgement

We gratefully acknowledge the support of the French “Agence Nationale pour la Recherche” (ANR n° ANR-07-PCVI-0032), for financing part of these researches.

Appendix A. Supplementary data

Supplementary data associated with this article can be found, in the online version, at doi:10.1016/j.talanta.2011.02.028.

References

[1] R. Wilson, Chem. Soc. Rev. 37 (2008) 2028–2045.
[2] E. Boisselier, D. Astruc, Chem. Soc. Rev. 38 (2008) 1759–1782.
[3] D. Astruc, E. Boisselier, C. Ornelas, Chem. Rev. 110 (2010) 1857–1959.
[4] R. Sardar, A.M. Funston, P. Mulvaney, R.W. Murray, Langmuir 25 (2009) 13840–13851.
[5] D. Tang, R. Yuan, Y. Chai, Y. Fu, J. Dai, Y. Liu, X. Zhong, Biosens. Bioelectron. 21 (2005) 539.
[6] Y.Y. Xu, C. Bian, S. Chen, S. Xia, Anal. Chim. Acta 561 (2006) 48–54.
[7] M.L. Mena, P. Yáñez-Sedeño, J.M. Pingarrón, Anal. Biochem. 336 (2005) 20–27.
[8] S. Xu, G. Tu, B. Peng, X. Han, Anal. Chim. Acta 570 (2006) 151–157.
[9] S. Mandal, S. Phadtare, M. Sasiry, Curr. Appl. Phys. 5 (2005) 118.
[10] L.A. Lyon, M.D. Musick, P.C. Smith, B.D. Reiss, D.J. Peña, M.J. Natan, Sens. Actuators B 54 (1999) 118–124.
[11] A.B.E.M.S. Azzam, O. Shekhah, A.R.E. Alawady, A. Birkner, C. Grunwald, C. Wöll, Thin Solid Films 518 (2009) 387–391.
[12] H.H. Tanaka, M. Isojima, T.H. Takeuchi, Colloids Surf., B: Biointerfaces 70 (2009) 259–265.
[13] A.L. Morel, R.M. Volmant, C. Methivier, J.M. Krafft, S. Boujday, C.M. Pradier, Colloids Surf., B: Biointerfaces 81 (2010) 304–312.
[14] K.N.J. Jung, J. Lee, Anal. Chim. Acta 651 (2009) 91–97.
[15] C.A. Mirkin, R.L. Letsinger, R.C. Micic, J.J. Storhoff, Nature 382 (1996) 607.
[16] D.S. Grubisha, R.J. Lipert, H.Y. Park, J. Driskell, M.D. Porter, Anal. Chem. 75 (2003) 5936–5943.
[17] J.D. Driskell, K.M. Kwarta, R.J. Lipert, M.D. Porter, Anal. Chem. 77 (2005) 6147–6154.
[18] S.C. Boca, C. Farcau, S. Astilean, Phys. Rev. B 267 (2009) 406–410.
[19] J. Turkevich, P.C. Stevenson, J. Hillier, Faraday Soc. 11 (1951) 55.
[20] K.C. Grabar, R.G. Freeman, M.B. Hommer, M.J. Natan, Anal. Chem. 67 (1995) 735–743.
[21] G. Frens, Nat. Phys. Sci. 241 (1973) 20–22.
[22] S. Boujday, C. Méthivier, B. Beccard, C.M. Pradier, Anal. Biochem. 387 (2009) 194–201.
[23] J.H. Scofield, J. Electron Spectrosc. Relat. Phenom. 8 (1976) 129.
[24] M. Wirde, U. Gelius, L. Nyholm, Langmuir 15 (1999) 6370–6378.
[25] D.G. Castner, K. Hinds, D.W. Grainger, Langmuir 12 (1996) 5083–5086.
[26] J.H. Fendler, Chem. Mater. 13 (2001) 3196–3210.
[27] A. Michota, A. Kudelski, J. Bukowska, Langmuir 16 (2000) 10236–10242.
[28] V.V. Tacabara, I.R. Nabiev, A.V. Feofanov, Langmuir 14 (1998) 1092–1098.
[29] A. Bonifacio, L. van der Sneppen, C. Gooijer, G. van der Zwan, Langmuir 20 (2004) 5858–5864.

[30] A. Kudelski, W. Hill, Langmuir 15 (1999) 3162–3168.
[31] C.H. Munro, W.E. Smith, M. Garner, J. Clarkson, P.C. White, Langmuir 11 (1995) 3712–3720.
[32] P.N. Njoki, I.I.S. Lim, D. Mott, H.-Y. Park, B. Khan, S. Mishra, R. Sujakumar, J. Luo, C.-J. Zhong, J. Phys. Chem. C 111 (2007) 14664–14669.
[33] C.J. Orendorff, A. Gole, T.K. Sau, C.J. Mutphy, Anal. Chem. 77 (2005) 3261.
[34] A.L. Morel, R.M. Volmant, C. Méthivier, J.M. Krafft, S. Boujday, C.M. Pradier, Colloids Surf. B: Biointerfaces 81 (2010) 304–312.
[35] S. Boujday, A. Bantegnie, E. Briand, P.G. Marnet, M. Salmain, C.M. Pradier, J. Phys. Chem. B 112 (2008) 6708–6715.
[36] M.P. Schwartz, S.D. Alvarez, M. Sailor, Anal. Chem. 79 (2007) 327.
[37] M.G. Gore, A.G. Popplewell, W.F. Ferris, M. Scawen, T. Atkinson, Biochem. Soc. Trans. 20 (1992) 289S.
[38] J. Pribyl, M. Hepel, J. Halamek, P. Skladal, Sens. Actuators B: Chem 91 (2003) 333–341.
[39] M.Z. Atashbar, B. Bejcek, A. Vijh, S. Singamaneni, Sens. Actuators B 107 (2005) 945.